J. Microelectromech. Syst., Vol. 15, No. 5, (2006), pp. 1364-1370.

Micromachined High-Aspect-Ratio Parylene Spring and Its Application to Low-frequency Accelerometers

Yuji Suzuki, *Member IEEE*, *Member ASME,* and Yu-Chong Tai, *Fellow, IEEE*

***Abstract*—A new microfabrication technology for high-aspect-ratio parylene structure has been developed for soft spring applications. Free-standing parylene beams with widths of 10-40 μm and aspect ratios of 10-20 have been successfully fabricated. Since parylene has a small Young's modulus, a high-aspect-ratio beam with a spring constant of the order of $1x10^{-3}$ N/m has been realized. The large yield strain of parylene enables a test structure to have a large-amplitude oscillation of 600 μm_{p-p}, without any failure of the high-aspect-ratio springs. An early prototype of in-plane capacitive accelerometer was also developed. It was found that its resonant frequency is as low as 37Hz, and the noise spectral density is 64 $\mu g/(Hz)^{0.5}$.**

***Index Terms*—parylene, low spring constant, high-aspect-ratio beam, capacitive accelerometer**

I. Introduction

For mechanical transducers with a high sensitivity, a soft beam with a low spring constant is required. However, since conventional MEMS materials such as single crystal Si have a large Young's modulus, it is not a straightforward process to develop soft structures. Weigold et al. [1] developed a Si accelerometer with a low spring constant of 0.127 N/m. However, very thin beams of 1 μm in width and 450 μm in length were required. An alternative approach for producing a soft spring is to use photosensitive polymer materials [2]-[4]. Lee et al. [4] employed SU-8 to make a cantilever beam for atomic force microscopy with a spring constant of 0.248 N/m. However, SU-8 is not suitable for mechanical structures requiring high accuracy due to its large internal stress and a relatively large thermal coefficient of expansion (TCE) of $5x10^{-5}$/K.

Manuscript received May 18, 2005; revised January 20, 2006. Subject Editor R. R. A. Syms. This work was the NSF Engineering Research Center (ERC) at Caltech.

Y. Suzuki is with the Department of Mechanical Engineering, the University of Tokyo, Tokyo 113-8656, Japan (phone: +81-3-5841-6411; fax: +81-3-5802-8858; e-mail: ysuzuki@thtlab.t.u-tokyo.ac.jp).

Y.-C. Tai is with the Electrical Engineering, California Institute of Technology, Pasadena, CA91125, USA.

Parylene (poly-para-xylylene) is known as a MEMS-compatible polymer that can be deposited with a CVD process, and is now attracting increasing attention for possible use in mechanical and fluidic micro devices [5]-[12]. Its physical properties and detailed internal stress characteristics have previously been reported [13], [14]. The advantage of using parylene for mechanical parts is three-folds; Firstly, parylene has a small Young's modulus (~ 4 GPa), which makes it easy to design soft springs with. Secondly, parylene is a non-brittle material with a large linear-elastic range (yield strain ~ 3%), which allows a large deflection without failure. Thirdly, parylene has a 30% lower TCE than SU-8 or polyimide.

The final goal of the present study is to develop micro-fabrication technology to be used to produce soft springs for in-plane transducers such as accelerometers [15]-[20] and energy harvesting devices [21], [22]. For these devices, sensitivity to mechanical force should vary by orders of magnitude depending on the direction. The structure should be soft in the direction of interest, but at the same time, it should be rigid in the other two perpendicular directions to minimize mechanical cross-talk. Therefore, high-aspect-ratio structures (HARS) are required.

The most straightforward approach to achieve HARS is to use deep reactive-ion etching (DRIE) of a Si substrate, such as the Bosch process [23]. HEXSIL [24], [25] and HARPSS [26] have also been proposed for high-aspect structures, where deep trenches are refilled with poly-Si. However, both single crystal Si and poly-Si are brittle, so mechanical failure is of considerable concern. Alternatively, high-aspect-ratio metal structures can be fabricated by the LIGA [27] process, but it requires X-ray, which is generally a much more expensive process. Moreover, all the existing technologies use materials with a large Young's modulus, which is larger than 100 GPa.

The objectives of the present study are to develop a new micro-fabrication technology for high-aspect-ratio parylene beams with a small spring constant, and to characterize their mechanical performance. We also present the first in-plane accelerometer using the parylene high-aspect-ratio beams.

II. Fabrication Of Parylene High-Aspect-Ratio Structures

The main process flow for the high-aspect-ratio parylene beam fabrication is shown in Fig. 1. The process starts with 4" Si wafers with 2 µm-thick thermal oxide. The upper SiO_2 is patterned with buffered HF (Fig. 1a) for the etch mask of DRIE, and 300-400 µm-deep trenches are etched into the substrate (Fig. 1b). The trenches are used as parylene molds and their depth defines the desired height of the beams. After stripping away the remaining SiO_2, a second 2 µm-thick thermal oxide is grown on all exposed Si surfaces as the etch-stop layer for the later DRIE (Fig. 1c). This is followed by a parylene-C deposition with a thickness of 10-20 µm to refill the trenches (Fig. 1d); the deposition pressure is chosen as 22 mT. The parylene film is then etched back using O_2 plasma (Fig. 1e). Next, the wafer is flipped over and etch windows are patterned into the backside SiO_2 with buffered HF (Fig. 1f). After dicing the wafer into individual die, each die is glued onto a support wafer, and the silicon is etched away from the backside with DRIE to expose the parylene beams, which are covered by the etch-stop SiO_2 (Fig. 1g). Finally, the beams are completely freed by stripping the SiO_2 away with buffered HF (Fig. 1h).

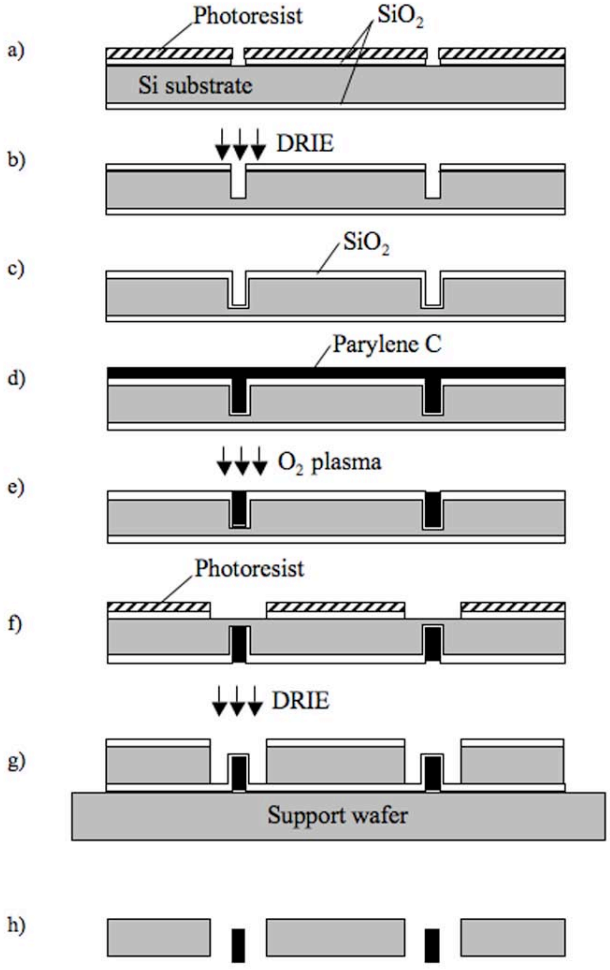

Fig. 1. Process flow for the high-aspect-ratio parylene structure. a) Wet oxidation and patterning SiO_2, b) Etch trench by DRIE, c) Stripping SiO_2 and making the second wet oxidation, d) Deposit of 20 µm-thick parylene-C, e) Etch-back parylene with O_2 plasma, f) Pattern SiO_2 on the backside of the wafer, g) Gluing onto a support wafer and etching through using DRIE, h) Stripping SiO_2 and the release of parylene structures with buffered HF.

Figure 2(a) shows an SEM image of a 20 µm-wide trench as deposited. Clearly, the parylene-C deposition is conformal, and the film thickness is almost uniform even inside the deep trench. This is because the mean free path of parylene molecules is as small as a few cm, and also because the sticking coefficient, which is defined by the ratio between the number of molecules reacting with a radical chain end and the number of incident monomer molecules onto the surface, is as low as $1x10^{-4}$ at room temperature [28].

Also visible is a small void inside, which is often observed in parylene deposition onto trenches [29]. The void is caused because the top part of the trench is sealed at an early stage of the deposition. The timing when the top part of the trench is

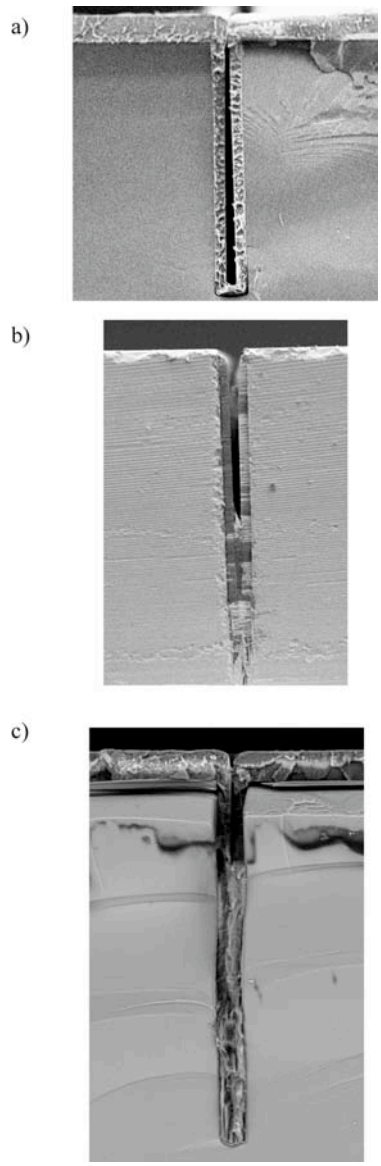

Fig. 2. Cross-sectional SEM images of a 20 µm-wide trench. a) As deposited, b) After the etchback, c) After the second deposition of 20 µm-thick parylene-C.

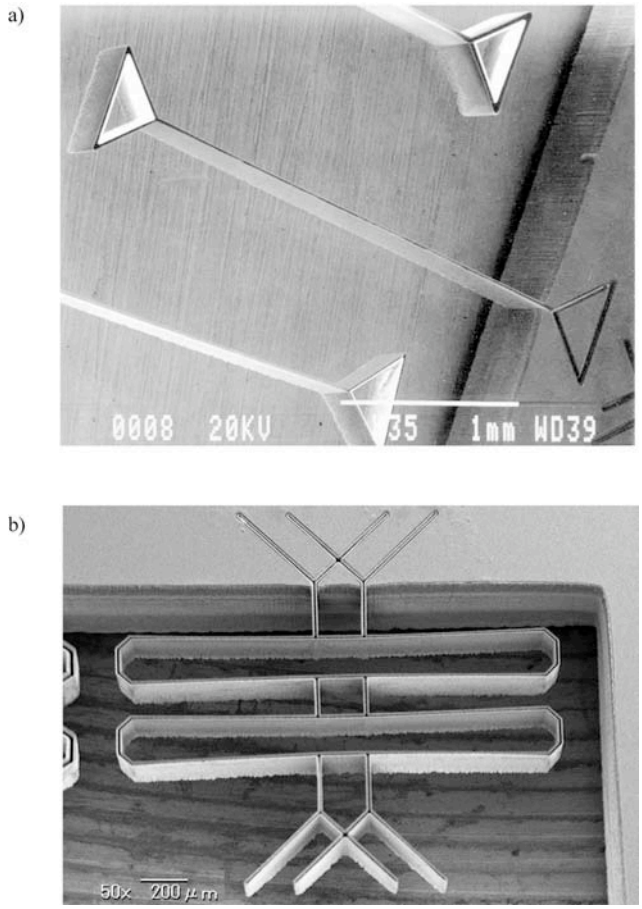

Fig. 3. SEM images of high-aspect-ratio free-standing parylene structures. a) Cantilever beam 30 µm in width, 400 µm in height and 2.5 mm in length, b) Leaf spring structure using a parylene beam 20 µm in width and 350 µm in height.

sealed with parylene depends on the trench width, and the time duration before the trench is sealed multiplied by the deposition rate determines the film thickness inside the trench. For 40 µm-wide trenches, the film thickness inside is about 17 µm. The film thickness inside the trench decreases with the trench width, and becomes 10 µm, 7 µm and 2.5 µm, respectively for 30 µm-, 20 µm-, and 10 µm-wide trenches.

After etch-back of the parylene film with O_2 plasma, the top part of the trench is opened (Fig. 2b). If desirable, this void can be completely eliminated with a second parylene-C deposition (Fig. 2c). The maximum aspect ratio fabricated here was 20, but trenches with higher aspect ratios can also be filled with parylene, once the trench itself is etched with DRIE.

Figure 3(a) shows an SEM image of a free-standing cantilever beam 30 µm in width, 400 µm in height, and 2.5 mm in length (aspect ratio of 13.3). A triangle-shaped trench etched into the substrate works well as an anchor. Figure 3(b) shows a leaf spring structure with an aspect ratio of 17.5. Si islands surrounded by parylene beam are successfully etched out with DRIE, and only free-standing complex parylene structures remain.

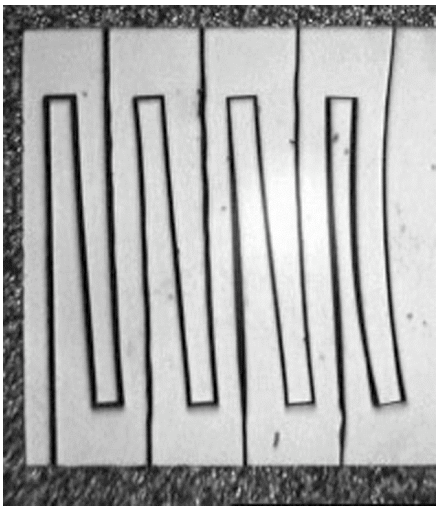

Fig. 4. Beam structures under tensile stress. Left to right, 40, 30, 20, and 10 µm-wide beam structures.

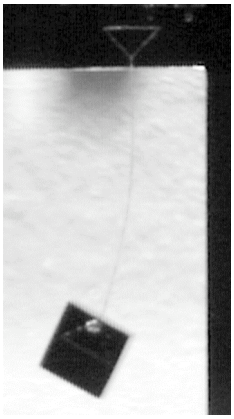

Fig. 5. A pendulum structure with a 10 µm-wide beam suspending 700 µm x 700 µm Si substrate under a gravity force.

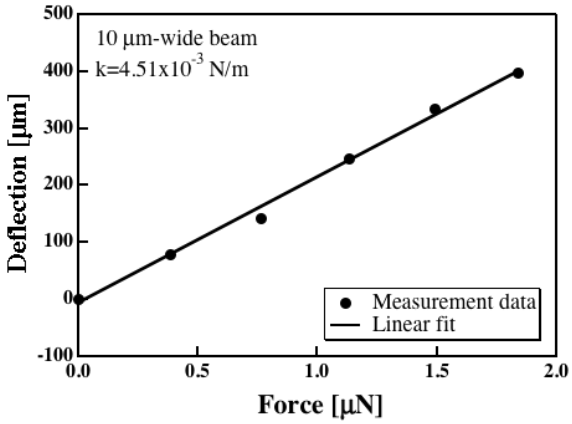

Fig. 6. Spring constant measurement of a 10 µm-wide beam.

Figure 4 shows parylene high-aspect-ratio beams of 10-40 µm in width. The 30 µm- and 40 µm-wide beams are 400 µm high, and the 10 µm- and 20 µm-wide beam structures are respectively about 200 µm and 350 µm in height due to the RIE lag. Parylene film is known to be in compressive stress as

it is deposited, but that becomes tensile stress after thermal annealing [13], [14]. In the present study, the parylene film undergoes baking at 100-110°C for the lithography step of the etch windows on the backside (Fig. 1f), and the beams are actually in tensile stress when released.

It is now clear that complex high-aspect-ratio parylene structures with aspect ratios up to 20 can be successfully fabricated through the present MEMS process. Static and dynamic characteristics of the structures are discussed in the next chapter.

III. Evaluation of Parylene High-Aspect-Ratio Beam

Figure 5 shows a magnified view of a pendulum structure with a 10 µm-wide beam, of which the aspect ratio is 20. The Si mass dimensions are 700 µm x 700 µm x 530 µm. The device was fixed onto a gonio stage, and the force in the in-plane direction is changed by altering the tilt angle. Figure 6 shows the deflection of the cantilever beam versus the force in the in-plane direction. It was discovered that the spring constant is as low as 0.0045 N/m. The spring constant obtained is 3 times smaller than the value estimated with conventional beam theory. This is probably because the trench is not fully-filled with parylene as shown in Fig. 2(b), and the cross section of the beams is U-shaped. On the other hand, this soft spring is robust and will not fracture even by shaking vigorously.

The spring constant for thicker beams was estimated from measurements of their resonant frequency. The measured values are respectively 0.0261, 0.169, and 0.484 N/m for 20 µm-, 30 µm-, and 40 µm-wide beams. Again, the measurement results are 3-7 times smaller than the designed values using the beam theory.

In order to study the dynamic response of parylene beams, test structures with a 1.75 mm x 1.75 mm Si proof mass, supported by two parylene leaf springs (Fig. 7a), were fabricated. Figure 8 shows the experimental setup. The device was glued onto a loud speaker and shaken in the in-plane direction at prescribed frequencies and amplitudes. Relative displacement of the proof mass to the substrate was measured visually using a CCD camera equipped with a high-magnification lens. Since the framing speed of the CCD camera is much slower than the oscillation frequency, the amplitude of the proof mass is measured from the streak length of the surface pattern as shown in Fig. 7(b). The resolution of the present amplitude measurement is one pixel of the image, which corresponds to about 3 µm.

Figure 9 shows the dynamic response of a proof mass with 20 µm-wide springs. The measurement data fit well with a simple spring-mass-damper model. The resonant frequency f_{res} and the quality factor Q are determined by a curve fit, and they are 112.9 Hz and 15.1, respectively. The peak-to-peak amplitude at the resonance is as large as 600 µm. The spring constant of each leaf spring structure is 0.9 N/m. The resonant frequencies for 30 µm-, and 40 µm-wide beams are respectively 257 and 410 Hz.

Figure 10 shows a snap-shot of the test structures at the oscillation frequency of 257 Hz. Only the structure with 30

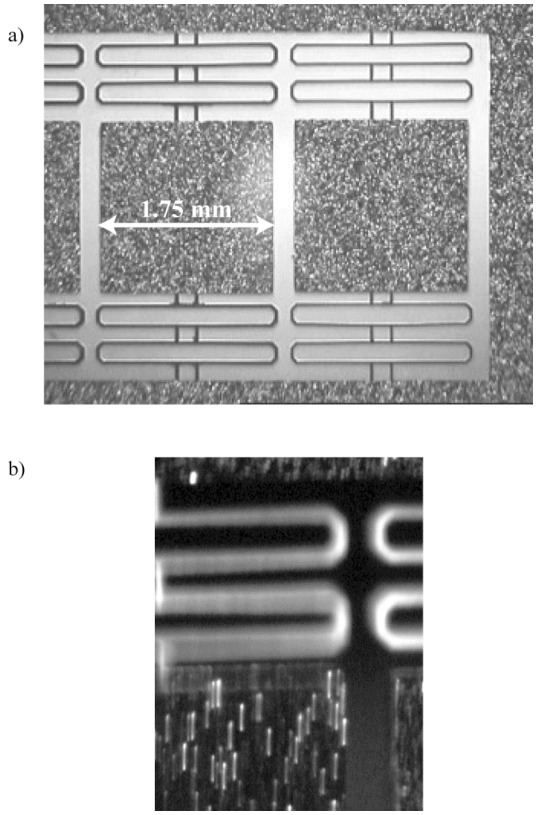

Fig. 7. Test structures with two high-aspect-ratio leaf springs and a 1.75 mm x 1.75 mm mass in between, as seen from the unpolished side. a) Left to right: 40 µm-, 30 µm-, and 20 µm-wide leaf springs. b) Magnified view of the proof mass in oscillation.

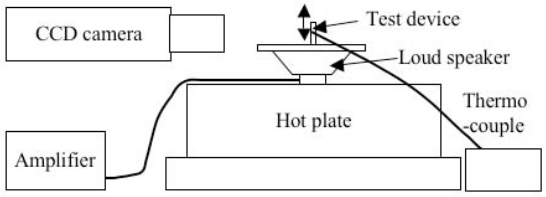

Fig. 8. Schematic of the experimental setup for the dynamic response measurement.

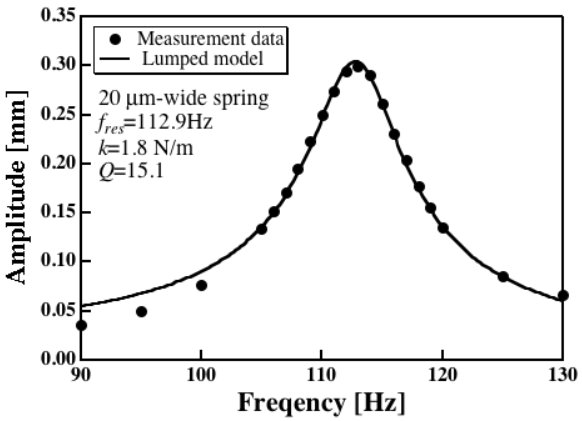

Fig. 9. Frequency response of the test structure with 20 µm-wide high-aspect-ratio leaf springs.

μm-wide springs is resonating. Because of the large oscillation amplitude, beams on the shrunk side are almost attached to each other. However, the springs undergo neither any damage nor plastic deformation. It is noted that the resonant frequency of these leaf springs remains unchanged even after being driven at their resonant frequency oscillation for several hours, which corresponds to about $2x10^6$ cycles. These findings confirm the robustness of parylene beams because of its large yield strain.

The effect of temperature on the spring constant of the high-aspect-ratio parylene springs was also examined. The device temperature was measured with a thermocouple, and ramped at about 1 ˚C /min. with a hot plate as shown in Fig. 8. Figure 11 shows the resonant frequency and the spring constant of the test structure with 40 μm-wide leaf-sprngs versus the temperature. The vertical axis is normalized at a value of 25 ˚C . It was found that the resonant frequency decreases monotonically with temperature at a rate of about 0.3 %/ ˚C , and is reduced by 21 % at 80 ˚C . This corresponds to the reduction of the spring constant at 0.6 %/ ˚C . Therefore temperature correction will probably be necessary for sensor applications. It is noted that this change in the spring constant is reversible; a spring constant at the same temperature remains unchanged even after several thermal cycles between room temperature and 80 ˚C , which is slightly lower than the glass transition temperature of parylene-C of 80-100 ˚C .

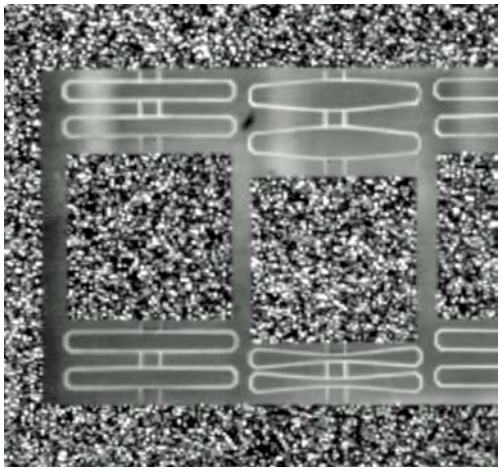

Fig. 10. A snap shot of the test structure with 30 μm-wide high-aspect-ratio leaf springs at the resonant frequency (~257 Hz). Left to right: 40 μm-, 30 μm-, and 20 μm-wide leaf springs.

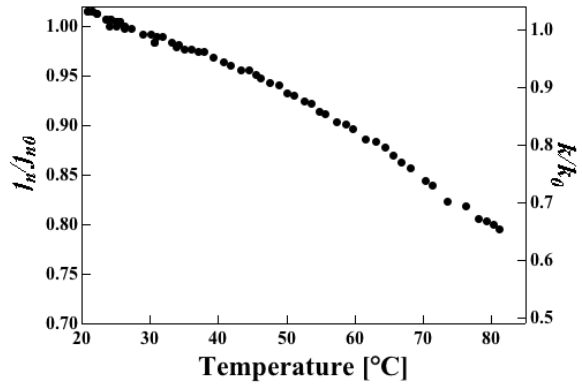

Fig. 11. The effect of temperature on the resonant frequency of the test structure using 40 μm-wide leaf springs. Vertical axis on the right represents the normalized spring constant.

IV. Prototype In-Plane Accelerometer

In order to demonstrate the advantages of the parylene high-aspect ratio beam, a prototype in-plane capacitive accelerometer was designed and fabricated. As shown in Figs. 12(a), (b), a proof mass (9.4 mm x 6 mm) was supported by four leaf springs. The beam width and height were 20 μm and 400 μm, respectively. In order to measure the displacement of

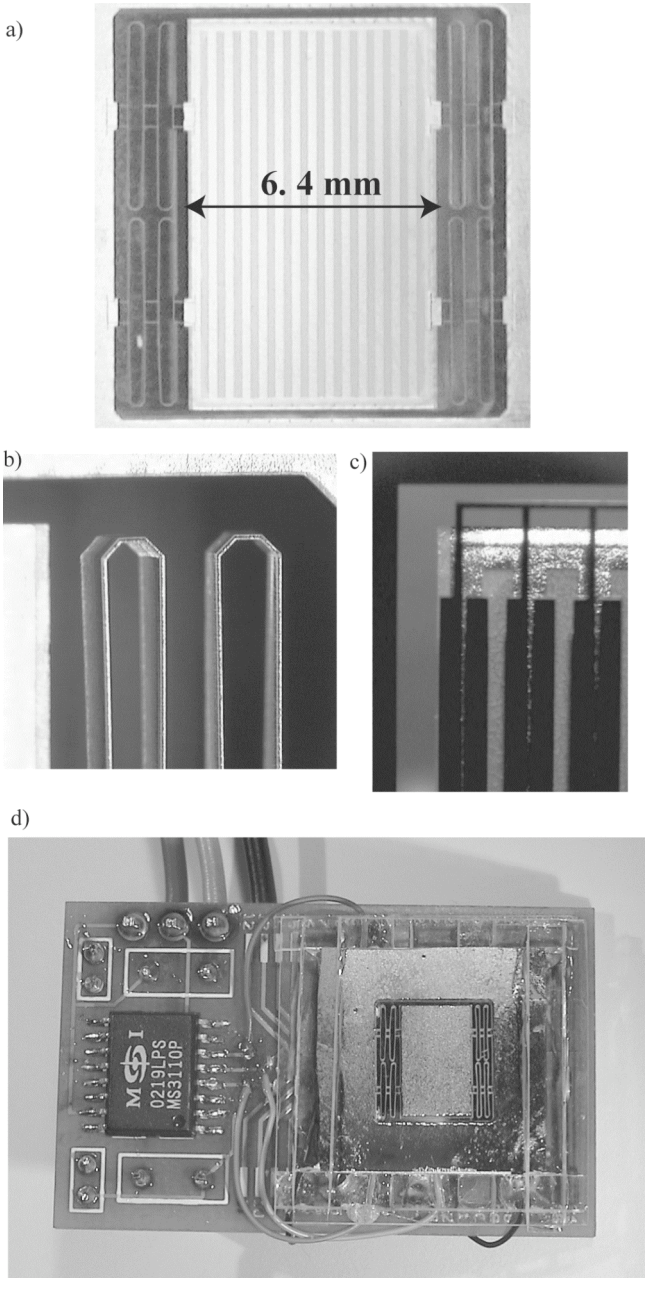

Fig. 12. Prototype of an in-plane capacitive accelerometer using high-aspect-ratio parylene springs. a) Proof mass with grid electrodes and leaf springs, b) Magnified view of the leaf spring (20 μm wide, 400 μm high), c) Magnified view through the counter electrode, d) Prototype device with a readout IC.

the proof mass with the capacitance change, grid electrodes were formed on the proof mass. Electrical contact between the proof mass and the external circuit was made through the parylene high-aspect- ratio beam. For this purpose, a second parylene deposition and etch-back were carried out in order to completely fill the void in the deep trench as shown in Fig. 2(c). After the second etch-back, a Cr/Au/Cr layer (100A/1000A/100A) is thermally- deposited and patterned on the top of the 20 μm-wide beams. Another a parylene film of 2 μm in thickness was deposited on the top of the electrode as a protection layer. Width and spacing of the grid electrodes were 200 μm. The resistance between the substrate and the grid electrodes was 60 Ω. The resonant frequency measured was 37 Hz, which is in good agreement with the designed value of 35 Hz, as the trenches are fully-filled with parylene.

The device chip with the proof mass was assembled with a glass chip with interdigitized counter electrodes as shown in Fig. 12(c). Figure 12(d) shows the early prototype accelerometer, in which a differential-type readout IC (MicroSensors Inc., MS3110) with a low noise floor of 4 aF/(Hz)$^{0.5}$ was used. Figure 13 shows the circuit diagram of the present system.

Since it was difficult to precisely control the gap between the electrodes on the proof mass and the counter electrodes, the gap is as large as 100 μm. In this configuration, the mechanical sensitivity, which is the theoretical capacitance change to the in-plane acceleration, is 4.5 pF/g. Thus the present prototype has almost the same sensitivity as the low-noise in-plane Si accelerometer developed by Chae et al.[20]

Figure 14 shows the static response of the accelerometer to

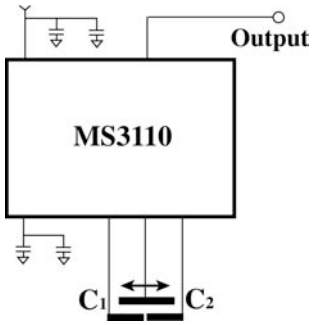

Fig. 13. Circuit diagram.

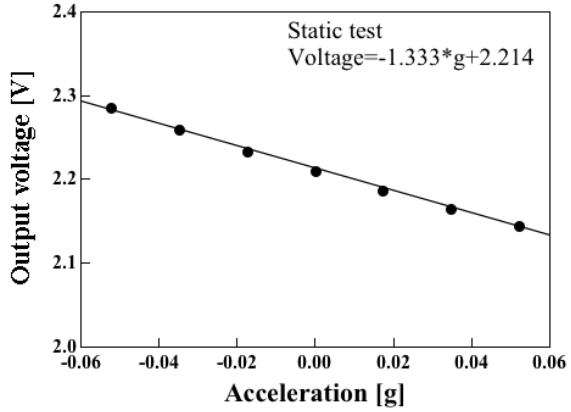

Fig. 14. Static response of the prototype accelerometer.

gravity by changing the tilt angle with respect to the gravitational direction. The overall sensitivity of this prototype was found to be -1.333 V/g, which is seven times smaller than the designed value. This is because the electrical sensitivity is poor; in the present design, the electrode width is only twice as large as the gap, so that a large fringe field should exist. Moreover, there is no guard electrode on the proof mass, which results in large parasitic capacitance.

It was also found that the noise floor of the present device was about 85 μV/(Hz)$^{0.5}$, which results in the noise spectral density of 64 μg/(Hz)$^{0.5}$, i.e., 6.3x10^{-4} m/s^2(Hz)$^{0.5}$. Therefore, whereas the present accelerometer is still an early prototype, it already has a low-noise floor, aided by the low spring constant of the parylene beam. Note that the noise floor is about ten times larger than that of the readout IC at 8.4 μV/(Hz)$^{0.5}$.

The Brownian equivalent acceleration noise $g_{n,B}$ is given by

$$g_{n,B} = (8\pi kT f_{res}/MQ)^{0.5}/g, \quad [\mathrm{g/(Hz)^{0.5}}] \qquad (1)$$

where k, T, and M are respectively the Boltzman constant, temperature, and the weight of the proof mass [30]. In the present accelerometer, f_{res} = 37 Hz, which is the lowest resonant frequency among MEMS accelerometers ever built. Futhermore, the mass M = 66 mg is much larger than that of previous MEMS accelerometers. As a result, $g_{n,B}$ as given by Eq. (1) is as low as 25 ng/(Hz)$^{0.5}$ or 2.5x10^{-7} m/s^2(Hz)$^{0.5}$, which is three orders of magnitude smaller than the noise floor measured.

Since the noise level of the present accelerometer is not

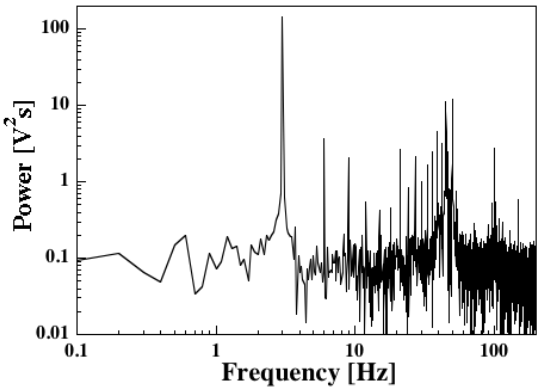

Fig. 15. Power spectra of output voltage for sinusoidal oscillation at 3 Hz.

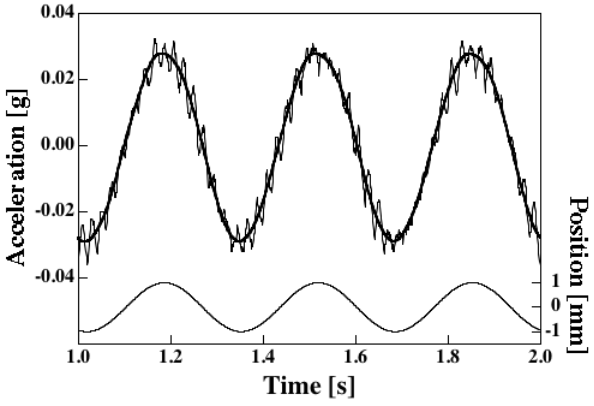

Fig. 16. Time trace of measured acceleration with sinusoidal oscillation at 3 Hz. The thick line represents filtered acceleration with a numerical low-pass filter at 20 Hz.

limited by Brownian noise, there exists considerable room to improve its sensitivity, especially the electrical sensitivity. For instance, when the gap between electrodes is reduced to 20 μm to suppress the fringe field, and the guard electrodes are formed on the proof mass to minimize the parasitic capacitance, the electrical sensitivity will jump to 48 V/g, which reduces the noise floor down to 1.8 $\mu g/(Hz)^{0.5}$.

The dynamic response of the prototype was examined in a preliminary experiment. The prototype was fixed onto the moving stage of a shaker (Labworks Inc., LW-140-110), and shaken in the in-plane direction. The oscillation of the stage was measured with a laser displacement meter (Keyence Corp., LC-2440), and the output voltage of the readout IC is digitized with a 14-bit AD converter. Figure 15 shows power spectra of the output voltage for a sinusoidal oscillation at 3 Hz. A sharp peak at the oscillation frequency can be observed. Since the present accelerometer is an under-damped system, a large peak is also observed at the resonant frequency.

Figure 16 shows a time trace of the acceleration measured. Sinusoidal oscillations at 3 Hz, having peak-to-peak amplitude of approximately 2 mm, are imposed, and the voltage output is converted into the acceleration using the static response shown in Fig. 14. An acceleration of around 50 mg_{p-p} at 3 Hz was successfully measured with the present prototype. Since the raw voltage signal includes fluctuations at the resonant frequency, a low-pass filter in Fourier space with a cut-off frequency of 20 Hz is used to remove the resonant frequency oscillation. The filtered data are also shown in Fig. 16, which are in good agreement with the imposed acceleration.

V. Conclusions

A new micro-fabrication technology for high-aspect-ratio parylene structure has been developed for soft spring applications, and its mechanical response has been fully characterized in a series of experiments. An early prototype in-plane accelerometer has been developed using parylene high-aspect-ratio springs. The following conclusions can be derived;

i) Free-standing parylene beams 10-40 μm in width with an aspect ratio of 10-20 can be fabricated.

ii) A high-aspect-ratio beam with a spring constant of 0.0045 N/m has been developed.

iii) In-plane oscillations with an amplitude as large as 600 μm_{p-p} has been achieved without any failure of the high-aspect ratio springs.

iv) An early prototype of an in-plane capacitive accelerometer with a record-low resonant frequency of 37 Hz has been developed. It has also been demonstrated that the prototype accelerometer can measure acceleration of 50 mg peak-to-peak amplitude at 3 Hz with a noise spectral density of 64 $\mu g/(Hz)^{0.5}$.

Acknowledgement

YS acknowledges Professor N. Kasagi in the University of Tokyo for his support during the course of this work.

References

[1] J. W. Weigold, K. Najafi, and S. W. Pang, "Design and fabrication of submicrometer, single crystal Si accelerometer," *J. Microelectromech. Syst*., vol. 10, pp. 518-524, 2001.

[2] G. Genolet, M. Despont, P. Vettiger, D. Anselmetti, and N. F. de Rooij, "All-photoplastic, soft cantilever cassette probe for scanning force microscopy," *J. Vac. Sci. Technol*., B, vol. 18, pp. 617-620, 2000.

[3] N. Chronis, and L. P. Lee, "Polymer MEMS-based microgripper for single cell manipulation," *Proc. 17th IEEE Int. Conf. MEMS*, Maastricht, pp. 17-20, 2004.

[4] J. Lee, H. Shin, S. Kim, S. Hong, J. Chung, H. Park, and J. Moon, "Fabrication of atomic force microscope probe with low spring constant using SU-8 photoresist," *Jpn. J. Appl Phys*., vol. 42, pp. L1171-1174, 2003.

[5] X. Xing, J. M. Yang, Y.-C. Tai, and C.-M. Ho, "Micromachined membrane particle filters," *Sensors and Actuators, A*, vol. 73, pp. 184-191, 1999

[6] L. Kicklider, X.-Q. Wang, A. Desai, Y.-C. Tai, and T. D. Lee, "A micromachined chip-based electrospray source for mass spectrometry," *Anal. Chem*., vol. 72, pp. 367-375, 2000.

[7] T. N. Pornsin-sirirak, Y.-C. Tai, H. Nassef, and C.-M. Ho, "Titanium-alloy MEMS wing technology for a micro aerial vehicle application," *Sensors and Actuators, A*, vol. 89, pp. 95-103, 2001.

[8] H. S. Noh, P. J. Hesketh, and G. C. Frye-Mason, "Parylene gas chromatographic column for rapid thermal cycling," *J. Microelectromech. Syst*., vol. 11, pp. 718-725, 2002.

[9] T.-J. Yao, X. Yang, and Y.-C. Tai, "BrF3 dry release technology for large freestanding parylene microstructures and electrostatic actuators," *Sensors and Actuators, A*, vol. 97, pp. 771-775, 2002.

[10] M. N. Niu, and E.-S. Kim, "Piezoelectric bimorph microphone built on micromachined parylene diaphragm," *J. Microelectromech. Syst*., vol. 12, pp. 892-898, 2003.

[11] J. Xie, J. Shih, Q. A. Lin, B. Z. Yang, and Y.-C. Tai, "Surface micromachined electrostatically actuated micro peristaltic pump," *Lab on Chip*, vol. 4, pp. 495-501, 2004.

[12] Z. Fan, J. M. Engel, J. Chen, and C. Liu, "Parylene surface-micromachined membranes for sensor applications," *J. Microelectromech. Syst*., vol. 13, pp. 484-490, 2004.

[13] S. Dabral, J. Vanetten, X. Zhang, C. Apblett, G. R. Yang, P. Ficalora, and J. F. McDonald, "Stress in thermally annealed Parylene films," *J. Electronic Materials*, vol. 21, pp. 989-994, 1992.

[14] T. A. Harder, T.-J. Yao, Q. He, C.-Y. Shih, and Y.-C. Tai, "Residual stress in thin-film Parylene-C," *Proc. 15th IEEE Int. Conf. MEMS*, Las Vegas, pp. 17-20, 2002.

[15] G. Schropfer, S. Ballandras, M. deLabachelerie, P. Blind, Y. Ansel, "Fabrication of a new highly-symmetrical, in-plane accelerometer structure by anisotropic etching of (100) silicon," *J. Micromech. Microeng*., vol. 7, pp. 71-78, 1997.

[16] Partridge, A., Reynolds, J. K., Chui, B. W., Chow, E. M., Fitzgerald, A. M., Zhang, L., Cooper, S. R., Kenny, T. W., and Maluf, N. I., "A high performance planar piezoresistive accelerometer," *Proc. Solid-State Sensor and Actuator Workshop*, Hilton Head, pp. 59-64, 1998.

[17] Lemkin, M. A., Juneau, T. N., Clark, W. A., Roessig, T. A., and Brosnihan, T. J., "A low-noise digital accelerometer using integrated SOI-MEMS technology," *Proc. 10th Int. Conf. Solid-State Sensors and Actuators (TRANSDUCERS '99)*, Sendai, pp. 1294-1297, 1999.

[18] Luo, H., Zhang, G., Carley, L. R., and Fedder, G. K., "A post-CMOS micromachined lateral accelerometer," *J. Microelectromech. Syst*., vol. 11, pp. 188-195, 2002.

[19] Jiang, X., Wang, F., Kraft, M., and Boser, B., "An integrated surface micromachined capacitive lateral accelerometer with 2ug/rtHz resolution," *Proc. Solid-State Sensors and Actuators Workshop*, Hilton Head, pp. 202-205, 2002.

[20] J. Chae, H. Kulah, K. Najafi, "An in-plane high-sensitivity, low-noise micro-g silicon accelerometer with CMOS readout circuitry," *J. Microelectromech. Syst*., vol. 13, pp. 628-635, 2004.

[21] P. D. Mitcheson, T. C. Green, E. M. Yeatman, and A. S. Holmes, "Architectures for vibration-driven micropower generators," *J. Microelectromech. Syst*., vol. 13, pp. 429-440, 2004.

[22] T. Tsutsumino, Y. Suzuki, N. Kasagi, and Sakane, Y., "Seismic power generator using high- performance polymer electret," *IEEE Int. Conf. MEMS 2006*, Istanbul, pp. 98-101, 2006.
[23] A. A. Ayon, R. Braff, C. C. Lin, H. H. Sawin and M. A. Schmidt, "Characterization of a time multiplexed inductively coupled plasma etcher," *J. Electrochem. Soc*., vol. 146, pp. 339-349, 1999.
[24] C. Keller, and M. Ferrari, "Milli-scale polysilicon structures," *Proc. Solid-state Sensor and Actuator Workshop*, Hiton Head, pp. 132-137, 1994.
[25] D. A. Horsley, M. B. Cohn, A. Singh, R. Horowitz and A. P. Pisano, "Design and fabrication of an angular microactuator for magnetic disk drives," *J. Microelectromech. Syst*., vol. 7, pp. 141-148, 1998.
[26] F. Ayazi and K. Najafi, "High aspect-ratio combined poly and single-crystal silicon (HARPSS) MEMS technology," *J. Microelectromech. Syst*., vol. 9, pp. 288-294, 2000.
[27] H. Guckel, "High-aspect-ratio micromachining via deep X-ray lithography," *Proc. IEEE*, vol. 86, pp. 1586-1593, 1998.
[28] Fortin, J. B., and Lu, T.-M., "A model for the chemical vapor deposition of poly(para-xylylene) (Parylene) thin films," *Chem. Mater*., vol. 14, pp. 1945-1949, 2002.
[29] Ilic, B., Czaplewski, D., Zalalutdinov, M., Schmidt, B., and Craighead, H.G., "Fabrication of flexible polymer tubes for micro and nanofluidic applications," *J. Vac. Sci. Technol., B*, vol. 20, pp. 2459-2465, 2002.
[30] J. Bernstein, R. Miller, W. Kelley and P. Ward, "Low-noise MEMS vibration sensor for geophysical applications," *Proc. Solid-State Sensor and Actuator Workshop*, Hilton Head, pp. 55-58, 1998.

Yuji Suzuki (M'01) received the B.S., M.S., and Dr. Eng. degrees in mechanical engineering from the University of Tokyo in 1987, 1989, and 1993, respectively. After spending one year at Nagoya Institute of Technology as a Assistant Professor, he joined Graduate School of Engineering at the University of Tokyo.

He is currently an Associate Professor in the Department of Mechanical Engineering at the University of Tokyo. His research interests include power MEMS such as MEMS energy harvesting devices, active flow control with MEMS sensors and actuators, and micro thermofluids systems such as micro catalytic combustor and MEMS cell sorting systems.

Yu-Chong Tai (M'97–SM'03-F'06) received the B.S. degree from National Taiwan University and the M.S. and Ph.D. degrees in electrical engineering from the University of California at Berkeley in 1986 and 1989, respectively.

After Berkeley, he joined the faculty of Electrical Engineering at the California Institute of Technology and built the Caltech Micromachining laboratory. He is currently a full Professor of Electrical Engineering at Caltech. His research interests include flexible MEMS, integrated microfluidics, neuroprobes and chips, optical MEMS and biochemical sensors.